Analyst

Cite this: *Analyst*, 2012, **137**, 4349

www.rsc.org/analyst

PAPER

Ultrasensitive electrochemical immunoassay based on graphene oxide–Ag composites for rapid determination of clenbuterol

Jing Bai, Yanjun Lai, Dawei Jiang, Yanbo Zeng, Yuezhong Xian,* Fei Xiao, Ningdan Zhang, Jie Hou and Litong Jin*

Received 9th April 2012, Accepted 22nd June 2012
DOI: 10.1039/c2an35473j

We report the development of an ultrasensitive amperometric biosensor based on Ag nanoparticles-decorated graphene oxide nanosheets (GO) (Ag–GO) for the rapid detection of clenbuterol (CLB). The morphology and structure of the Ag–GO labeled CLB (Ag–GO–CLB) were characterized by transmission electron microscope (TEM), atomic force microscope (AFM), and ultraviolet-visible spectroscope (UV-vis). The immunosensor was prepared by covalently immobilizing capture antibodies on a multi-walled carbon nanotubes-modified glassy carbon electrode. Through competitive immunoreactions, the Ag–GO–CLB nanocomposites were captured on the immunosensor and the silver was measured by positive differential pulse voltammetry (DPV) in KCl solution for the detection of antigen. The experimental results show a linear response over the range from 0.01 to 10.0 ng mL^{-1} with a lower detection limit of 6.8 pg mL^{-1} (signal-to-noise ratio of 3). The Ag–GO based immunosensor offers a simple and convenient route for metal-immunoassay labels, which can avoid the complicated and time-consuming dissolving of metal component for ultrasensitive determination. Moreover, the electrochemical immunoassay shows acceptable specificity and stability and is suitable for the determination of CLB in real samples.

Introduction

Graphene and its derivatives have attracted increasing attention in recent years as a novel class of 2D carbon-based nanomaterials.[1] It has been regarded as a 'next generation material' because of its remarkable electronic, optical, thermal, chemical and mechanical properties. Until now, graphene has been applied in both emerging and conventional fields such as field-effect transistors,[2] sensors,[3] electrochemical devices,[4–6] electromechanical resonators,[7] polymer nanocomposites,[8] batteries,[9] capacitors,[10] and light emitting devices.[11] Graphene oxide (GO), which was exfoliated from graphite with a mild ultrasonic treatment, bears lots of oxygen-containing functional groups.[12] The most widely accepted structure for GO is that of an extended graphene sheet decorated with hydroxyl and epoxy functional groups on the basal plane and carboxyl and carbonyl groups at the edges.[13] GO has been proved to possess overwhelming physical/chemical properties and has been applied in a variety of fields, which have been reviewed by several authors, for example, Dreyer *et al.*,[14] Rao *et al.*,[15] and Yang *et al.*[16] As a novel carbon material, graphene and GO are highly expected as a substitute for CNTs to provide an effective platform for developing hybrid materials because of their large interfacial surface area and low price.[17] Furthermore, the presence of oxygen containing groups can provide a handle for the chemical modification of GO using well-developed carbon surface chemistry. For example, GO has been used as a nanoscale building block to anchor metal ions to form hybrid materials.[18] Varieties of nanoparticles (NPs), such as Pd, Pt and quantum dots, have been used to decorate graphene sheets, which provides a new way to develop catalytic, magnetic, and optoelectronic materials.[19] Dong's group successfully synthesized graphene/platinum hybrid nanostructures by alternatively assembling ionic liquid-modified graphene nanosheets and platinum NPs.[20] Jafri *et al.* fabricated an electrochemical sensor for oxygen reduction by using nanostructured Pt dispersed on graphene-multiwalled carbon nanotube hybrid nanomaterials.[21]

As one of the members of the noble metallic nanomaterials family, Ag NPs exhibit the highest thermal and electrical conductivity and have been widely used in electronics, photonics, biological labelling, and surface-enhanced Raman scattering (SERS).[22] For example, Seong and co-workers reported that silver NPs were deposited on SWCNTs films using the electrochemical patterning technique for the detection of H_2O_2.[23] Yang *et al.* demonstrated that Ag NPs were self-assembled into nanochains for surface-enhanced Raman scattering.[24] Ag–GO nanocomposites have been synthesized and used as antibacterial materials[25] and SERS substrates. For example, Ma *et al.* reported the deposition of Ag nanoparticles on the surface of modified

Department of Chemistry, East China Normal University, 3663 Zhongshan Road(N), Shanghai, 200062, P.R.China. E-mail: ltjin@chem.ecnu.edu.cn; yzxian@chem.ecnu.edu.cn; Fax: +86-21-62232627; Tel: +86-21-62232627

GO nanosheets and an antibacterial mechanism was proposed to understand the superior antibacterial activity of the Ag–GO composite.[26] Zheng and co-workers developed the photo-induced process to *in situ* growth of Ag NPs on the surface of GO to produce graphene oxide–Ag nanocomposites and applied it as a SERS substrate.[27] Wang's group fabricated graphene oxide/Ag nanoparticle hybrids according to a self-assembly procedure and used the obtained GO/PDDA/AgNPs as SERS substrates.[28] Furthermore, much interest also has been paid on the fabrication of biosensors based on Ag–GO nanocomposites due to their two-dimensional structure and unique properties. Wan *et al.* studied graphene oxide sheet-mediated silver enhancement for application to electrochemical biosensors and the use of graphene oxide as a promoter for Ag(I) reduction was also exploited for colorimetric detection.[29] Qu *et al.* reported an electrochemical immunosensor for the detection of protein biomarker platelet-derived growth factor BB (PDGF-BB) based on graphene oxide (GO) initiated silver enhancement.[30] However, considering these results, despite the significant efforts, there still exist some challenges and information regarding electrochemical studies on Ag–GO based composites is still insufficient.

Clenbuterol is a β-adrenergic agonist, which is used in human and veterinary medicine as a therapeutic drug for pulmonary disease.[31,32] CLB can accelerate animal growth[33] and produce more muscle and much less adipose tissue. However, the residues of CLB in meat can lead to food poisoning. Symptoms from CLB residue-induced food poisoning have been reported from investigations of separate events in several countries.[34] Moreover, drug residues may negatively impact the export trade of edible animal products and result in nearly incalculable economic loss. Therefore, the use of CLB has been banned in most countries and it is crucial to develop a simple, fast and portable method for analysis of CLB. At present, several techniques have been developed to detect CLB, including confirmatory methods and screening methods.[35,36] The confirmatory methods such as gas chromatography-mass spectroscopy,[37] liquid chromatography-mass spectroscopy.[38] Both of them require extensive sample clean-up and complicated testing processes.[39] The screening methods are often immunoassays[40] which provide the advantages of sensitivity, specificity and user-friendly analysis. Recently, electrochemical immunosensors have attracted growing attention because they combine the high specificity of traditional immunoassay with the low detection limits and low price of electrochemical measurement. Previously, studies on immunosensors have mainly focused on protein or microbe detection. These targets have multiple recognition sites and can be detected by conventional sandwich immunoassay. However, for small molecules, such as clenbuterol, the sandwich structure is improper because of its small-size and non-multiple recognition sites. Until now, few works have been done to develop electrochemical immunosensors,[41,42] it is crucial to develop a simple, fast and sensitive method for the analysis of CLB.

In this work, a competitive electrochemical immunoreaction system based on Ag–GO nanocomposites is developed for the rapid and ultrasensitive detection of CLB (Scheme 1). Ag–GO nanocomposites are prepared by *in situ* reduction of silver ions in exfoliated graphite oxide, in which GO is prepared by oxidizing graphite according to the modified Hummer's method[43–45] and employed as a nanocarrier for Ag NPs. The resulting Ag–GO nanocomposites are further used as a tag to label CLB *via* an amidization reaction (Scheme 1A). A competitive immunoreactions system is developed so that Ag–GO labeled CLB (Ag–GO–CLB) competes with free CLB in the solution through specific antigen–antibody reaction with the monoclonal antibody to CLB (anti-CLB) immobilized on a carboxylated multi-wall carbon nanotubes (MWCNTs)-modified glassy carbon electrode (GCE) (Scheme 1B). The quantity of immuno-conjugated antigen could be detected based on the differential pulse voltammetric (DPV) response of the labeled Ag NPs (Scheme 1C). To the best of our knowledge, this is the first time that Ag NPs-decorated GO was used as a label in immunoassay for CLB detection. Compared with conventional immunoassay, this protocol offers several advantages, such as simple preparation, fast response, especially the elimination of the direct redox reaction in PBS. Some amperometric immunosensors place the redox in PBS such as $[Fe(CN)_6]^{3-/4-}$, Prussian blue to produce the direct electrochemical signals. However, these techniques necessitate an additional step of the target involvement that increases the analysis time and complexity. The functional Ag–GO nanocomposites have the capability for metal ion chelation and biomolecular immobilization and are expected to have potential applications in immunoassay.

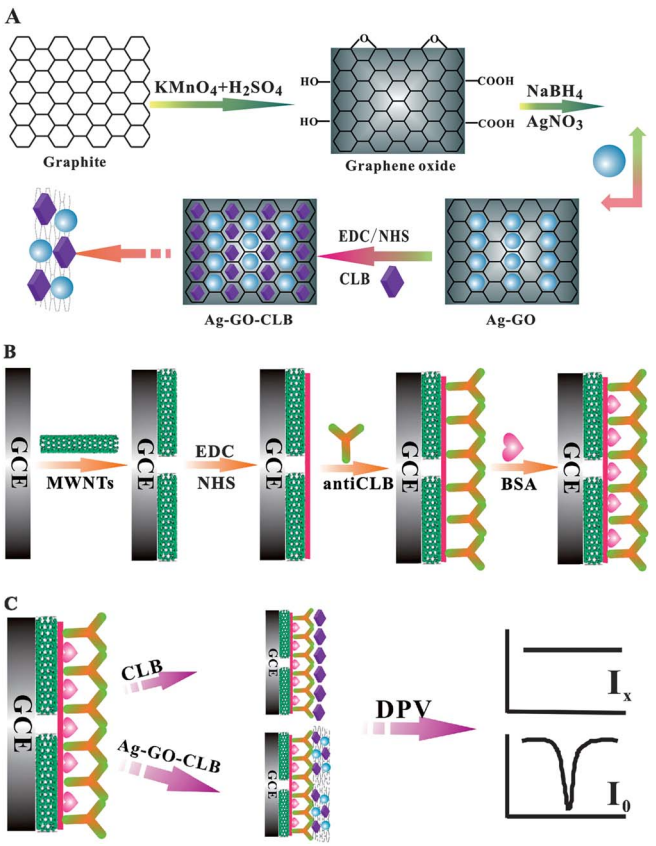

Scheme 1 (A) Schematic representation of preparation of Ag–GO–CLB conjugates, (B) preparation of immunosensors and (C) competitive-type electrochemical immunoassay.

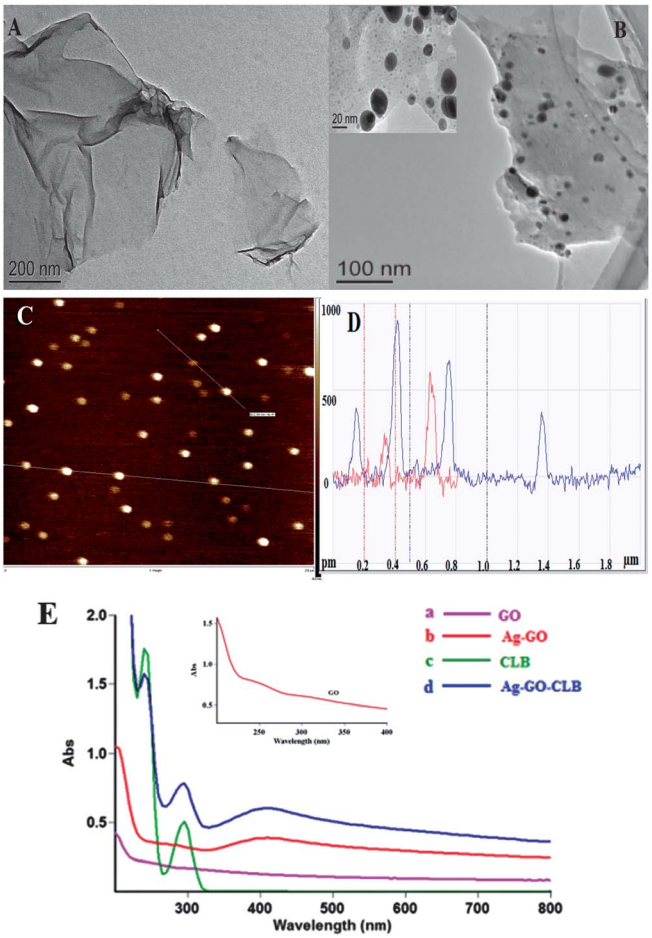

Fig. 1 TEM images of (A) GO, and (B) Ag-decorated GO. AFM image of (C) GO and the height profiles (D) along the line shown in the AFM image. (E) UV-vis spectra of (a) GO, (b) Ag–GO, (c) CLB and (d) Ag–GO–CLB conjugate respectively.

Experimental

Materials and apparatus

Anti-CLB was purchased from Guangzhou Ucando Biotechnology (Guangzhou, China). CLB, MWCNTs (50 nm in diameter, 1–2 μm in length), bovine serum albumin (BSA), 1-ethyl-3-(3-dimethylaminopropyl)carbodiimide hydrochloride (EDC), and *N*-hydroxysuccinimide (NHS) were purchased from Sigma-Aldrich (USA). Graphite, sodium borohydride ($NaBH_4$), silver nitrate ($AgNO_3$), and sodium hydroxide (NaOH) were purchased from Shanghai Chemical Factory (Shanghai, China). Phosphate-buffered saline (PBS buffer, 10 mM, pH = 7.4) was prepared by varying the ratio of NaH_2PO_4 and Na_2HPO_4. All the reagents used were of analytical reagent grade and all solutions were prepared with pure water from Millipore (Milli-Q, 18.2 MΩ cm^{-1}).

The morphologies of GO and Ag–GO were characterized with a JEM-2000 transmission electron microscope (TEM) (JEOL, Japan). The ultraviolet-visible (UV-vis) absorption spectra of the GO and Ag NPs were recorded with a Cary 500 UV-vis-NIR spectrometer (Varian, USA). All the electrochemical measurements were carried out on a CHI 660C electrochemical workstation (CHI, USA) with a three-electrode system, an anti-CLB/MWCNTs/GCE as working electrode, a saturated calomel electrode (SCE) as reference electrode and a platinum electrode as counter electrode.

Preparation of GO

GO was synthesized based on the modified Hummer's method.[46–48] Briefly, 0.5 g graphite, 0.5 g $NaNO_3$ and 3.0 g $KMnO_4$ were slowly added to 25 mL concentrated H_2SO_4 under vigorous stirring at 0 °C. The mixture was then stirred for 1 h below 35 °C to oxidize the graphite. After that, 40 mL distilled water was added into the mixture and the temperature was increased to 90 °C, and the suspension was maintained at 95 °C for 15 min. The mixture was then poured into 100 mL distilled water, then, 3 mL H_2O_2 was added into the suspension. After cooling to room temperature, the resulting mixture was washed by repeated centrifugation and filtration, with 5% HCl aqueous solution and distilled water. The remaining dark-yellow solid was dried under vacuum at 40 °C for 48 h.[49] The obtained materials were dispersed in water to yield a yellow-brown suspension (1 mg mL^{-1}) for further usage.

Preparation of Ag–GO–CLB conjugates

The preparation of Ag–GO–CLB is shown in Scheme 1A. Firstly, Ag–GO was prepared by *in situ* reduction of silver ions in exfoliated GO dispersions. Typically, 4 mL of solution of GO (1 mg mL^{-1}) was mixed well with 5 mL $AgNO_3$ (0.1 M) and the pH of the resulting suspension was adjusted to 10.0 by NaOH. Subsequently, 10 mL $NaBH_4$ (0.6 mM) was added under vigorous stirring at room temperature for 1 h. The resulting Ag–GO hybrid material was purified by centrifugation and redispersed in water. For the synthesis of Ag–GO–CLB conjugates, CLB was attached to Ag–GO using an EDC/NHS amidization protocol. Briefly, 0.5 mL Ag–GO conjugates were mixed with 800 mM EDC (250 μL) and 200 mM NHS (250 μL) in 1.0 mL PBS and activated for 1 h. The mixture was centrifuged at 15 000 rpm for 10 min and the supernatant was discarded. The wash was repeated to remove excess EDC and NHS. Subsequently, the resulting Ag–GO was dispersed in 1.0 mL PBS (pH = 7.4) and sonicated for 5 min to obtain a homogeneous dispersion. Then, 50 μL CLB (0.1 mg mL^{-1}) was added to the solution of Ag–GO and gently mixed overnight at room temperature. The reaction mixture was then centrifuged at 15 000 rpm for 10 min and the supernatant was removed. Bovine serum albumin (BSA) was used to block uncovered spaces on the Ag–GO surface. Ag–GO–CLB conjugates were treated with 1 mL 5% BSA solution for 30 min to block non-specific binding. The mixture was centrifuged using PBS to remove any free CLB and BSA. The final mixture was redispersed in 1.0 mL PBS (pH = 7.4) and stored at 4 °C before use.

Preparation of CLB immunosensor

To fabricate the sensor of anti-CLB/MWNTs/GC electrode, MWCNTs-COOH was prepared. Briefly MWCNTs were dispersed in concentrated hydrochloric acid for 24 h, then centrifuged and washed with distilled water more than 3 times until the pH was neutral, the mixture was then sonicated in a

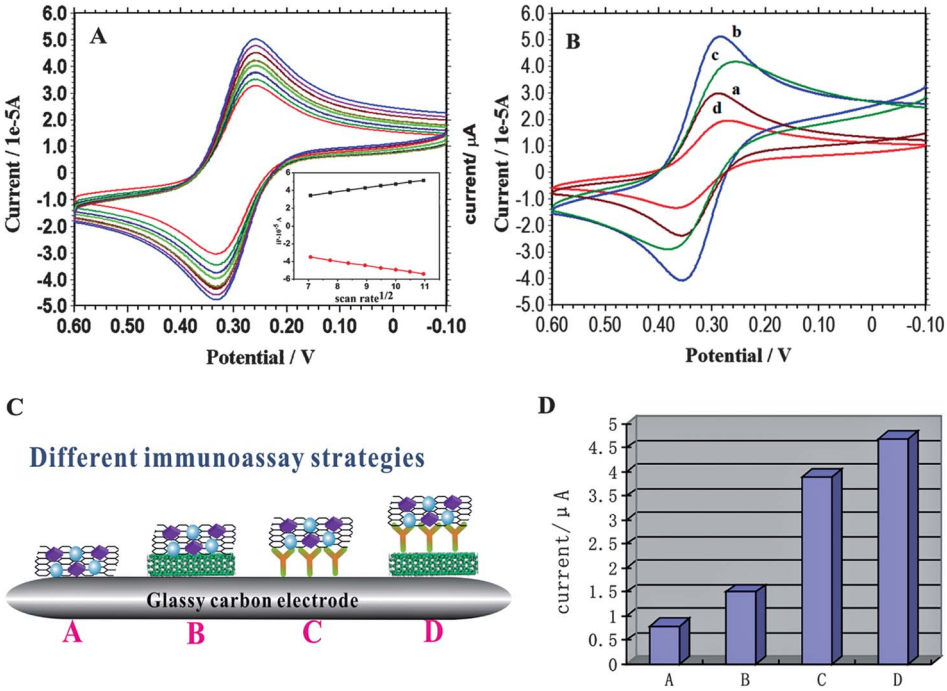

Fig. 2 (A) Cyclic voltammograms of the MWCNTs-modified GCE with scan rates from 50 to 120 mV s^{-1} in $[Fe(CN)_6]^{3-/4-}$. The inset of the panel shows the dependence of peak currents on the square root of the scan rates. (B) Cyclic voltammograms of the electrode in the presence of $[Fe(CN)_6]^{3-/4-}$ (scan rate 100 mV s^{-1}): (a) bare GCE; (b) after modified with MWCNTs; (c) after antibody immobilization; (d) after CLB binding. (C) Schematic representations of four types of electrochemical immunoassay strategies. (D) Column chart of the DPV peak currents for different immunoassay strategies.

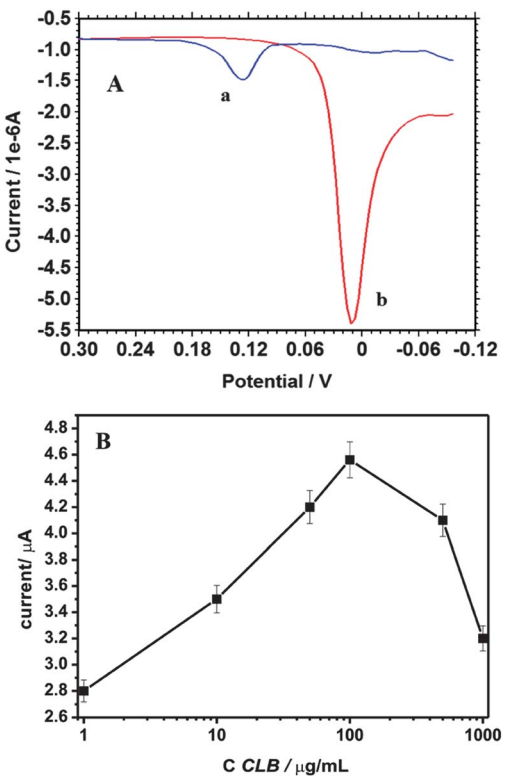

Fig. 3 Effect of analytical solution (a) KNO_3, (b) KCl (A), concentrations of Ag–GO–CLB on DPV peak currents ($n = 5$) (B).

mixture of concentrated HNO_3 and H_2SO_4 (v/v, 1 : 3) for 6 h. The resulting dispersion was centrifuged and washed repeatedly with distilled water until the pH was about 7.0. This procedure can remove metallic and carbonaceous impurities, and generate carboxylated groups on the MWCNTs. Prior to the surface modification, the bare GCE was sequentially polished with 0.05 and 1.0 μm alumina slurry, and then washed ultrasonically in distilled water and ethanol for 10 min, respectively.

For immunosensor fabrication (Scheme 1B), typically, 10 μL of MWCNTs-COOH dispersions was spread on the surface of the GCE, and then dried at room temperature for 1 h. After rinsing thoroughly with PBS, the MWCNTs films were formed on the surface of the GCE. Then the MWCNTs-COOH-modified GCE was treated with 0.8 M EDC and 0.1 M NHS for 0.5 h to convert the terminal carboxylic group to the active NHS ester. After rinsing with water and PBS, 2 μL of 0.75 mg mL^{-1} anti-CLB was added dropwise to the electrode and incubated at 37 °C for 2 h. Subsequently, the formed anti-CLB/MWNTs-modified GCE was rinsed with PBS and incubated in 1.0% BSA solution for 0.5 h at 37 °C to eliminate non-specific binding and block the remaining active groups. After rinsing with PBS, the immunosensor was stored at 4 °C when not in use.

Amperometric immunosensing of CLB

A competitive immunoassay was conducted for the detection of CLB (Scheme 1C). Briefly, 2 μL of Ag–GO labeled CLB was mixed with different concentrations of free CLB, and then the final volume was made up to 10 μL by PBS buffer and sonicated for 5 min to obtain a homogeneous dispersion. The electrode

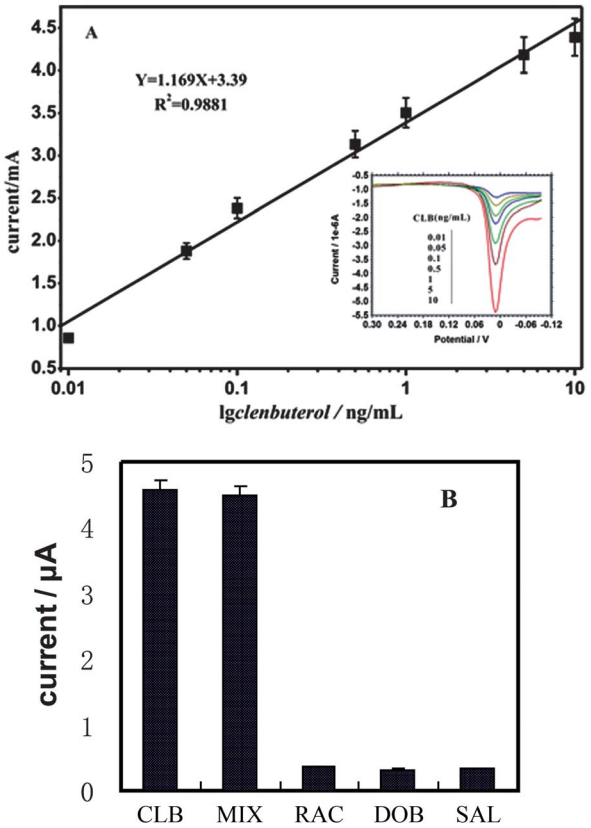

Fig. 4 (A) Calibration curves of the immunosensor for CLB determination in 1.0 M KCl. The inset is the DPV response of different concentrations of CLB from 0.01 to 10 ng mL^{-1} ($n = 7$). (B) Specificity investigation of the immunosensor for CLB (0.1 mg mL^{-1}) and interferents mixtures with CLB (0.1 mg mL^{-1}): ractopamine (RAC) (0.1 mg mL^{-1}), (c) dobutamine (DOB) (0.1 mg mL^{-1}), (d) salbutamol (SAL) (0.1 mg mL^{-1}).

modified with anti-CLB/MWCNTs was further incubated with 10 μL of the mixed solution for 1 h at 37 °C to complete the competitive immunoreaction. After washing with PBS to remove the non-specific adsorption of conjugates, the electrochemical detection was performed in a 10 mL analytical cell containing 1.0 M KCl as the electrolyte solution. The captured Ag through antigen–antibody reaction was determined based on the DPV scanning from −0.1 to +0.3 V.

Results and discussion

Characterization of Ag–GO–CLB nanoconjugate

Fig. 1A and B show typical TEM image of GO, and Ag–GO nanocomposites. As can be seen in Fig. 1A, layer-structured GO with a smooth surface is obtained. While the GO was decorated with Ag NPs by the reduction of silver ions *in situ* in exfoliated GO dispersions, there is a homogeneous and dense coverage of Ag NPs on the GO surface. Fig. 1B shows a uniform surface topography and the diameter of Ag NPs is about 20 nm. In addition, no aggregation of GO sheets or Ag NPs is observed. Fig. 1C and D display the typical AFM images of GO and height profiles along the line shown in the AFM image. The height profiles distribution shows that the thickness of GO is about 0.9 nm, which is characteristic of fully exfoliated graphene sheets and agrees well with the observations in the TEM images. To further investigate the interaction of the nanoconjugate of Ag–GO–CLB, the UV-vis absorption spectra of GO, Ag–GO, CLB antigen and Ag–GO–CLB conjugate were studied, respectively (Fig. 1E). Prior to the UV-vis measurements, the samples were dispersed in water by sonication. The spectroscopic response of GO solution shows a weak absorption band at 236 nm, whereas Ag NPs exhibit a distinct surface plasmon absorption band with the maximum absorbance at about 410 nm. When Ag NPs were deposited onto GO, the absorbance at 410 nm can be observed (curve b), confirming the formation of Ag–GO. It could be seen that CLB displays two absorption peaks at 243 and 296 nm (curve c), respectively. When CLB was bound to Ag–GO *via* the EDC/NHS reaction, three absorption peaks are observed (curve d), indicating the successful binding of CLB to Ag–GO.

Principle of the electrochemical immunoassay

The fundamentals of the electrochemical immunoassay based on the Ag–GO–CLB conjugate for CLB detection are illustrated in Scheme 1C. The detection principle of the immunosensor is based on the competition between free CLB in samples and Ag–GO–CLB conjugates for the limited anti-CLB on the immunoelectrode surface. Anti-CLB was assembled onto MWCNTs to form a ready-to-use immunoelectrode. After removal of the unbound molecule, Ag NPs in the conjugates were reduced to the ionic Ag^+ in a positive voltage and determined by DPV. Briefly, in the absence of free CLB, Ag–GO–CLB was mostly bound to monoclonal antibodies, which resulted in the maximum current I_0. In the presence of free CLB, Ag–GO–CLB was partly or not bound to monoclonal antibodies, which resulted in the decreased or blank current I_x. In any case, the current signal is inversely related to the CLB concentration in samples. The current signal for 0 ng mL^{-1} CLB is I_0, while I_x is for unknown samples or standard solutions, the current reduction ($\Delta I = I_0 - I_x$) is used for the CLB quantification.

Table 1 Recoveries of CLB from the spiked samples

	Immunosensor			ELISA			LC-MS		
Amount added/ mg kg^{-1}	Found/mg kg^{-1}	Recovery (%)	RSD (%)	Found/ mg kg^{-1}	Recovery (%)	RSD (%)	Found/ mg kg^{-1}	Recovery (%)	RSD (%)
5	4.56 ± 0.23	91.2	4.16	4.78 ± 0.19	95.6	4.26	4.65 ± 0.05	93.0	3.98
10	9.31 ± 0.16	93.1	5.28	10.16 ± 0.36	101.6	4.58	9.02 ± 0.23	90.2	4.19
20	18.29 ± 0.82	91.4	4.31	19.08 ± 1.09	95.4	3.64	17.98 ± 0.62	89.9	3.26

Electrochemical behaviour of the modified electrodes

The electrochemical behaviors of different electrodes were investigated by cyclic voltammetry (CV) using $K_3Fe(CN)_6$ as the redox probe. Fig. 2A depicts typical cyclic voltammograms of the MWCNTs-modified electrode in 5 mmol L^{-1} $K_3Fe(CN)_6$ with different scan rates. With increasing scan rate, the anodic and cathodic peak currents are linearly proportional to the square root of the scan rates ranging from 50 to 120 mV s^{-1}, indicating that the redox process is reversible and diffusion-controlled.[50] Fig. 2B shows the electrochemical responses of different electrodes in $K_3Fe(CN)_6$ solution. As shown in Fig. 2B, CV is performed from −0.1 to 0.6 V with a scan rate of 100 mV s^{-1} at room temperature. The cyclic voltammograms at the bare GCE exhibit a pair of stable and well-defined redox peaks for $Fe(CN)_6^{3-}$/$Fe(CN)_6^{4-}$. After modification with MWCNTs, the response is enhanced. While with further modification with anti-CLB, the redox peak current is decreased due to the blocking effect of anti-CLB. After incubating with Ag–GO–CLB, the CV response of the redox probe is further reduced, which may result from the introduction of CLB onto the electrode surface by the immunoreactions.

To further clarify the amplified properties of the electrochemical immunoassay using the synthesized Ag–GO–CLB nanoconjugate, four immunoassay strategies were utilized including Ag–GO–CLB immobilized onto a GCE *via* physical adsorption (Ag–GO–CLB/GCE), coupling reaction with MWCNTs (Ag–GO–CLB/MWCNTs/GCE), and antigen and antibody reaction without MWCNTs (Ag–GO–CLB/anti-CLB/GCE) and Ag–GO–CLB/MWCNTs/antiCLB/GCE). These immunoassay protocols are illustrated in Fig. 2C and abbreviated as sensors A, B, C and D. Based on the electrochemical response of sensors A and B (Fig. 2D), the use of MWCNTs could obviously enhance the signal of the electrochemical immunoassay. The reason might be the fact that MWCNTs not only obviously increased the amount of carboxyl groups for covalent coupling of more anti-CLB, but also accelerated the electron transfer. Moreover, the signal could further increase using the Ag–GO–CLB/anti-CLB/GCE immunoassay protocol. In contrast to sensors A and B, the sensitivity of sensor C is improved. It may be attributed to the good affinity between antibody and antigen and more Ag NPs were captured. As shown in Fig. 2D, sensor D exhibits the best performance, indicating that the amplified currents are not only derived from the specificity of the immunoreaction but also originated from the coated MWCNTs.

Optimization of conditions for electrochemical detection

Firstly, the temperature effect on the immunoreaction has been performed. The reaction of Ag–GO–CLB and antibody was examined at room temperature, 37 and 50 °C, respectively. The maximum response occurred at a reaction temperature of 37 °C, indicating that the antibody exhibits the highest affinity towards CLB at this temperature. Thus, 37 °C is selected as the optimum incubation temperature in this study. The incubation time is another important parameter for the specific recognition of Ag–GO–CLB. With incubation times of 20, 40, 60, 80 and 100 min, the electrochemical response increases with the increasing incubation time and tends to a steady value after 1 h, indicating a thorough capture of the antigens on the electrode surface. A longer incubation shows saturated binding sites between antigen and antibody and results in a large non-specific signal. Therefore, the optimal incubation time for immunoreactions is 1 h. We also investigated the effects of analytic solution and concentration of Ag–GO–CLB on the electrochemical response, which is shown in Fig. 3. The electrochemical detection was performed in a 10 mL analytical cell containing 1.0 M KCL and 0.6 M KNO_3 respectively (Fig. 3A). In comparison with the stripping peak current in KNO_3, the well-defined sharp stripping peak for silver is more favorable for the highly sensitive detection of CLB due to the Ag/AgCl solid-state voltammetric process in KCl.[51] The sensitivity of the immunosensor relies on the formation of the immunocomplex on the electrode which is dependent on the amount of CLB decorated on Ag–GO. More CLB molecules on the Ag–GO will generate more immunocomplexes and enhance the DPV intensity. However, an excessive amount of labeled CLB will weaken the absorption between Ag and GO and decrease the DPV signal (Fig. 3B). To obtain the best performance of the immunosensor, different concentrations of CLB decorated on Ag–GO were synthesized and used for the construction of the immunocomplex. As can be seen the maximal signal was achieved when the CLB concentration is 100 μg mL^{-1}. Thus, 100 μg mL^{-1} CLB was employed to synthesize the Ag–GO–CLB conjugates for the immunosensor construction.

Analytical performance characteristics

Under the optimized conditions, the electrochemical responses of the immunosensor for different concentrations of CLB are investigated. It can be seen that a linear relationship between the current ($\Delta I = I_0 - I_x$) and CLB concentration is obtained over the range from 0.01 to 10.0 ng mL^{-1} with a correlation coefficient of 0.9940. The detection limit is calculated to be 6.8 pg mL^{-1} based on 3σ of the blank signals, which is better than that of 0.32 ng mL^{-1} based on the label-free electrochemical immunosensor[37] and 0.1 ng mL^{-1} using the carbon nanotubes-based electrochemical immunosensor.[38]

To investigate the specificity of electrochemical immunosensor for real sample analysis, the interferences of ractopamine, dobutamine, and salbutamol are evaluated. As shown in Fig. 4B, no remarkable interference is found, which indicates that the immunosensor has good selectivity and is suitable for real sample analysis. The reproducibility of the immunosensor was further evaluated by intra- and inter-assay coefficients of variation. The intra-assay precision of the analytical method is 3.2% and 3.9% at 0.1 and 1.0 ng mL^{-1} CLB, respectively ($n = 6$). Similarly, the inter-assay coefficients of variation for six immunosensors are 4.1% and 4.7% at 0.1 and 1.0 ng mL^{-1} CLB, respectively. These results demonstrate acceptable reproducibility and precision. In addition, the immunosensor could be stored at 4 °C for 1 month without reducing the electrochemical response.

Detection of CLB in real samples

Recovery study was used to assess the accuracy of the immunosensor in real samples. Urine samples were obtained from the local market. All of the urine samples were filtered through

0.22 μm filter twice and then stored in the refrigerator at 4 °C when not in use. CLB standard solution was added to the blank urine samples and the resulting concentrations of CLB in the urine samples are 5, 10, and 20 mg kg^{-1}. For each sample, three methods were performed, including the amperometric immunosensor, ELISA and LC-MS. The results show that the electrochemical immunosensor has good consistency with ELISA and LC-MS. Accuracy was also evaluated by adding different amounts of CLB to urine samples and the recovery was measured. Recoveries for the same concentration by three different methods show no statistical differences, indicating a reasonable parallel and accuracy of the sensor when applied to real samples (Table 1).

Conclusions

In summary, an ultrasensitive and simple electrochemical immunosensor was developed for ultrasensitive CLB detection, in which Ag–GO nanocomposites were used as a tag for CLB labeling and enhanced sensitivity is achieved by using GO as a nanocarrier to immobilize CLB and Ag NPs. Based on a competitive immunoreaction strategy, the electrochemical immunosensor shows a linear response in the range of 0.1–10 ng mL^{-1} with a limit detection of 6.8 pg mL^{-1} (signal-to-noise ratio of 3). Due to the good precision, high sensitivity, acceptable stability and excellent selectivity, the electrochemical immunosensor has potential application for the rapid and simple measurement of CLB in real samples.

Acknowledgements

This work was supported by the National Natural Science Foundation of China (no. 21175046), New Century Excellent Talents in University (no. NCET-09-0357) and Open Foundation of Shanghai Key Laboratory of Green Chemistry and Chemical Process.

References

1 A. K. Geim and K. S. Novoselov, *Nat. Mater.*, 2007, **6**, 183–191.
2 X. Li, G. Zhang, X. Bai, X. Sun, X. Wang, E. Wang and H. Dai, *Nat. Nanotechnol.*, 2008, **3**, 538–542.
3 J. Lu, L. T. Drzal, R. M. Worden and I. Lee, *Chem. Mater.*, 2007, **19**, 6240–6246.
4 X. Wang, L. Zhi and K. Mullen, *Nano Lett.*, 2007, **8**, 323–327.
5 D. A. C. Brownson and C. E. Banks, *Analyst*, 2010, **135**, 2768–2778.
6 D. A. C. Brownson, L. J. Munro, D. K. Kampouris and C. E. Banks, *RSC Adv.*, 2011, **1**, 978–988.
7 J. S. Bunch, A. M. van der Zande, S. S. Verbridge, I. W. Frank, D. M. Tanenbaum, J. M. Parpia, H. G. Craighead and P. L. McEuen, *Science*, 2007, **315**, 490–493.
8 J. H. Jung, D. S. Cheon, F. Liu, K. B. Lee and T. S. Seo, *Angew. Chem.*, 2010, **49**, 5708–5711.
9 C.-H. Lu, H.-H. Yang, C.-L. Zhu, X. Chen and G.-N. Chen, *Angew. Chem.*, 2009, **48**, 4785–4787.
10 H. A. Godwin, *Curr. Opin. Chem. Biol.*, 2001, **5**, 223–227.
11 H. Needleman, *Annu. Rev. Med.*, 2004, **55**, 209–222.
12 J. Chattopadhyay, A. Mukherjee, C. E. Hamilton, J. Kang, S. Chakraborty, W. Guo, K. F. Kelly, A. R. Barron and W. E. Billups, *J. Am. Chem. Soc.*, 2008, **130**, 5414–5415.
13 H. C. Schniepp, J.-L. Li, M. J. McAllister, H. Sai, M. Herrera-Alonso, D. H. Adamson, R. K. Prud'homme, R. Car, D. A. Saville and I. A. Aksay, *J. Phys. Chem. B*, 2006, **110**, 8535–8539.
14 D. R. Dreyer, S. Park, C. W. Bielawski and R. S. Ruoff, *Chem. Soc. Rev.*, 2010, **39**, 228–240.
15 C. N. R. Rao, A. K. Sood, K. S. Subrahmanyam and A. Govindaraj, *Angew. Chem.*, 2009, **48**, 7752–7777.
16 W. Yang, K. R. Ratinac, S. P. Ringer, P. Thordarson, J. J. Gooding and F. Braet, *Angew. Chem.*, 2010, **49**, 2114–2138.
17 S. Stankovich, D. A. Dikin, G. H. B. Dommett, K. M. Kohlhaas, E. J. Zimney, E. A. Stach, R. D. Piner, S. T. Nguyen and R. S. Ruoff, *Nature*, 2006, **442**, 282–286.
18 D. W. Boukhvalov and M. I. Katsnelson, *J. Am. Chem. Soc.*, 2008, **130**, 10697–10701.
19 H. Bai, C. Li and G. Shi, *Adv. Mater.*, 2011, **23**, 1089–1115.
20 C. Zhu, S. Guo, Y. Zhai and S. Dong, *Langmuir*, 2010, **26**, 7614–7618.
21 R. I. Jafri, T. Arockiados, N. Rajalakshmi and S. Ramaprabhu, *J. Electrochem. Soc.*, 2010, **157**, B874–B879.
22 X. C. Song, Y. Zhao, Y. F. Zheng, E. Yang, J. Fu and Y. He, *Cryst. Growth Des.*, 2008, **8**, 1823–1826.
23 M.-P. N. Bui, X.-H. Pham, K. N. Han, C. A. Li, Y. S. Kim and G. H. Seong, *Sens. Actuators, B*, 2010, **150**, 436–441.
24 Y. Yang, J. Shi, T. Tanaka and M. Nogami, *Langmuir*, 2007, **23**, 12042–12047.
25 J. Shen, M. Shi, N. Li, B. Yan, H. Ma, Y. Hu and M. Ye, *Nano Res.*, 2010, **3**, 339–349.
26 J. Ma, J. Zhang, Z. Xiong, Y. Yong and X. S. Zhao, *J. Mater. Chem.*, 2011, **21**, 3350–3352.
27 J. Chen, X. Zheng, H. Wang and W. Zheng, *Thin Solid Films*, 2011, **520**, 179–185.
28 W. Ren, Y. Fang and E. Wang, *ACS Nano*, 2011, **5**, 6425–6433.
29 Y. Wan, Y. Wang, J. Wu and D. Zhang, *Anal. Chem.*, 2010, **83**, 648–653.
30 F. Qu, H. Lu, M. Yang and C. Deng, *Biosens. Bioelectron.*, 2011, **26**, 4810–4814.
31 C. Crescenzi, S. Bayoudh, P. A. G. Cormack, T. Klein and K. Ensing, *Anal. Chem.*, 2001, **73**, 2171–2177.
32 G. Degand, A. Bernes-Duyckaerts and G. Maghuin-Rogister, *J. Agric. Food Chem.*, 1992, **40**, 70–75.
33 C. T. Elliott, S. R. H. Crooks, J. G. D. McEvoy, W. J. McCaughey, S. A. Hewitt, D. Patterson and D. Kilpatrick, *Vet. Res. Commun.*, 1993, **17**, 459–468.
34 C. Pulce, D. Lamaison, G. Keck, C. Bostvironnois, J. Nicolas and J. Descotes, *Vet. Hum. Toxicol.*, 1991, **33**, 480–481.
35 G. Zhu, Y. Hu, J. Gao and L. Zhong, *Anal. Chim. Acta*, 2011, **697**, 61–66.
36 J. Kong, L. Jiang, X. Su, J. Qin, Y. Du and B. Lin, *Lab Chip*, 2009, **9**, 1541–1547.
37 G. Biancotto, R. Angeletti, P. Traldi and F. Guidugli, *J. Mass Spectrom.*, 1999, **34**, 1346–1353.
38 A. Aresta, C. D. Calvano, F. Palmisano and C. G. Zambonin, *J. Pharm. Biomed. Anal.*, 2008, **47**, 641–645.
39 M. H. A. Botterblom, M. G. P. Feenstra and E. B. H. W. Erdtsieck-Ernste, *J. Chromatogr., Biomed. Appl.*, 1993, **613**, 121–126.
40 W. Haasnoot, P. Stouten, R. Schilt and D. Hooijerink, *Analyst*, 1998, **123**, 2707–2710.
41 P. He, Z. Wang, L. Zhang and W. Yang, *Food Chem.*, 2009, **112**, 707–714.
42 G. Liu, H. Chen, H. Peng, S. Song, J. Gao, J. Lu, M. Ding, L. Li, S. Ren, Z. Zou and C. Fan, *Biosens. Bioelectron.*, 2011, **28**, 308–313.
43 S. Gilje, S. Han, M. Wang, K. L. Wang and R. B. Kaner, *Nano Lett.*, 2007, **7**, 3394–3398.
44 G. Eda, G. Fanchini and M. Chhowalla, *Nat. Nanotechnol.*, 2008, **3**, 270–274.
45 Y. Shao, J. Wang, M. Engelhard, C. Wang and Y. Lin, *J. Mater. Chem.*, 2010, **20**, 743–748.
46 W. S. Hummers and R. E. Offeman, *J. Am. Chem. Soc.*, 1958, **80**, 1339.
47 X. Sun, Z. Liu, K. Welsher, J. Robinson, A. Goodwin, S. Zaric and H. Dai, *Nano Res.*, 2008, **1**, 203–212.
48 S. Ge, M. Yan, J. Lu, M. Zhang, F. Yu, J. Yu, X. Song and S. Yu, *Biosens. Bioelectron.*, 2012, **31**, 49–54.
49 J. R. Lomeda, C. D. Doyle, D. V. Kosynkin, W.-F. Hwang and J. M. Tour, *J. Am. Chem. Soc.*, 2008, **130**, 16201–16206.
50 E. Laviron, *J. Electroanal. Chem. Interfacial Electrochem.*, 1979, **101**, 19–28.
51 B. P. Ting, J. Zhang, M. Khan, Y. Y. Yang and J. Y. Ying, *Chem. Commun.*, 2009, 6231–6233.